

Scattering properties of dark atoms and molecules

James M. Cline, Zuowei Liu, and Guy D. Moore

Department of Physics, McGill University, 3600 Rue University, Montréal, Québec H3A 2T8, Canada

Wei Xue

INFN, Sezione di Trieste, SISSA, via Bonomea 265, 34136 Trieste, Italy

(Received 4 December 2013; published 19 February 2014)

There has been renewed interest in the possibility that dark matter exists in the form of atoms, analogous to those of the visible world. An important input for understanding the cosmological consequences of dark atoms is their self-scattering. Making use of results from atomic physics for the potentials between hydrogen atoms, we compute the low-energy elastic scattering cross sections for dark atoms. We find an intricate dependence upon the ratio of the dark proton to the dark electron mass, allowing for the possibility to “design” low-energy features in the cross section. Dependences upon other parameters, namely the gauge coupling and reduced mass, scale out of the problem by using atomic units. We derive constraints on the parameter space of dark atoms by demanding that their scattering cross section not exceed bounds from dark matter halo shapes. We discuss the formation of molecular dark hydrogen in the Universe and determine the analogous constraints on the model when the dark matter is predominantly in molecular form.

DOI: [10.1103/PhysRevD.89.043514](https://doi.org/10.1103/PhysRevD.89.043514)

PACS numbers: 95.35.+d, 12.60.Cn

I. INTRODUCTION

Dark atoms are one of the oldest models of particle dark matter [1,2], originally suggested by the venerable idea of mirror symmetry [3–7]. More recently, the idea of dark sectors with gauge interactions not necessarily identical to those of the standard model has gained attention [8,9], motivating authors to take a fresh look at the implications of dark atoms [10–16]. Unlike dark matter consisting of elementary particles, dark atoms can have large self-interaction cross sections, which may impact the structure of galactic halo profiles, or those of clusters of galaxies, on which there are observational constraints.

A previous study [15] explored the impact of these constraints on the parameter space of a simple atomic dark matter (DM) model, making simplifying assumptions about the nature of the self-interaction cross section. In this paper we aim to avoid such assumptions and to thereby obtain more accurate predictions, while illustrating a rich range of possibilities for the energy dependence of the cross sections. If tentative evidence for significant dark matter self-interactions improves (for a recent review, see Ref. [17]), these features could prove useful for model building, as they allow one to construct scattering cross sections with intricate features appearing at energies much lower than would be possible in other theories of self-interacting dark matter.

We define the atomic DM model in Sec. II and review results from the atomic literature in the interaction potential between atoms in Sec. III. The methodology for computing scattering cross sections is presented in Sec. IV, and the resulting predictions for scattering lengths in the singlet and

triplet channels are given in Sec. V. We present the energy dependence of the atomic cross sections in Sec. VI. Constraints on the model from DM halo structure are derived in Sec. VII. In Sec. VIII we present analytic fits to the momentum-transfer cross section to facilitate the use of our results by the reader. The formation of dark molecules is discussed in Sec. IX, and the structure formation bounds analogous to those of atoms are given in Sec. X. We summarize and conclude in Sec. XI.

II. THE MODEL

We assume that dark atoms (**H**) are analogous to visible hydrogen, consisting of bound states of a fermionic dark electron **e** and proton **p** with masses m_e and m_p , respectively, and with equal and opposite charges under a dark electromagnetism with a massless dark photon and fine-structure constant α . (We do not refer to the usual fine-structure constant in this paper, so there will be no confusion between the two.) Otherwise, the physics need not be the same as in the visible sector, and in particular we do not assume that there are dark neutrons or nuclei. By definition, we take the dark electron to be the lighter of the two constituents. The dark hydrogen binding energy is given by $\alpha^2 \mu_{\mathbf{H}}/2$, where $\mu_{\mathbf{H}} = m_e m_p / (m_e + m_p)$ is the reduced mass. The atomic unit (a.u.) of energy is defined to be $\epsilon_0 = \alpha^2 \mu_{\mathbf{H}}$, while that of length is the Bohr radius, $a_0 = (\alpha \mu_{\mathbf{H}})^{-1}$. Sometimes we will omit the explicit writing of ϵ_0 and a_0 in the specification of energies or distances; in such cases the use of atomic units should be understood.

The model thus depends upon only three parameters, which can be taken as ϵ_0 , a_0 , and the ratio $R = m_p/m_e$. We

will see that the dependence of physical quantities on ϵ_0 and a_0 is trivial, if we ignore the contribution of the binding energy to the mass of the dark atom, $m_{\mathbf{H}} \cong m_{\mathbf{e}} + m_{\mathbf{p}}$. In this case they scale out of physical quantities by choosing atomic units, leaving only R as the relevant one to vary.

III. INTERATOMIC POTENTIALS

The electrons in the scattering \mathbf{H} atoms can be in the spin triplet or singlet states (which must be averaged over for unpolarized scattering). The interaction potential depends on the spin because the overall wave function must be antisymmetric. The singlet state has a symmetric spatial wave function, leading to a much deeper potential well, allowing two \mathbf{H} to bind into molecular \mathbf{H}_2 with binding energy $0.16\epsilon_0$ and bond length $1.4a_0$. (We are using the Born-Oppenheimer approximation, in which the electronic state is solved for at each value of the \mathbf{p} - \mathbf{p} separation, or equivalently, the \mathbf{e} 's respond adiabatically to the \mathbf{p} motion. This approximation is valid in a large- R expansion, and we will make it throughout.) The triplet state must have a spatially antisymmetric electronic wave function, leading to a potential with a very shallow minimum with energy $-2 \times 10^{-5}\epsilon_0$ at $r = 7.9a_0$. We plot them in Fig. 1 and explain their origin in the following.

The triplet potential V_t has been computed in Ref. [18], and an analytic fit to these results has been given [19] as

$$\frac{V_t}{\epsilon_0} = \exp(c_0 - c_1 r - c_2 r^2) - D(r) \left(\frac{c_6}{r^6} + \frac{c_8}{r^8} + \frac{c_{10}}{r^{10}} \right), \quad (1)$$

with $c_0 = 0.09678$, $c_1 = 1.10173$, $c_2 = 0.03945$, $c_6 = 6.5$, $c_8 = 124$, $c_{10} = 3285$, and $D(r) = \exp(-(r_1/r - 1)^2)$ if $r < r_1$ [$D(r) = 1$ otherwise], with $r_1 = 10.04$ in atomic units. The first term represents the repulsive exchange contribution, while the second models the attractive van der Waals part. We find that Eq. (1) gives a good fit to the

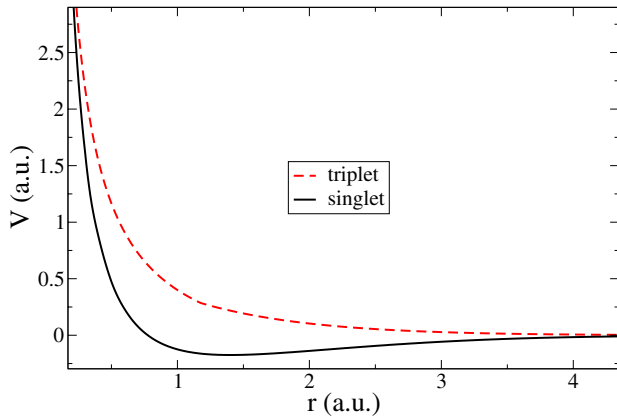


FIG. 1 (color online). Interaction potentials for hydrogen atoms with electrons in spin singlet or triplet states. Here and throughout, “a.u.” stands for “atomic units,” namely ϵ_0 for energy and a_0 for distance, as discussed in the text.

original data of Ref. [18] for $r > 1.176$, and we extrapolate to lower r using $V_t = -0.3652 + 0.7653/r$ for $r \leq 1.176$. (The r^{-1} behavior provides a smooth fit to the tabulated potential at small r .)

The singlet potential V_s has been computed more recently in Ref. [20], where results are tabulated in the range $0.2 < r < 12$. We interpolate between the tabulated values for $0.3 < r < 12$, and extrapolate to small r using $V_s = -1.5379 + 0.94714/r$ for $r \leq 0.3$. To extrapolate to $r > 12$, following Ref. [19], we have made a fit to $\ln(V_t - V_s)$ versus r , which turns out to be nearly linear in r in this region, thus obtaining $V_s = V_t - \exp(2.3048 - 1.6238r)$.

We have found that the predictions for scattering from these potentials are much more sensitive to small changes in V_s than to V_t , due to the deeper minimum in the former. It is therefore appropriate that more computational effort has been made in the atomic physics community to provide accurate recent determinations of V_s , while the existing form of V_t seems to be adequate. For example, Ref. [21] obtains a scattering length from the approximation in Eq. (1) that is consistent with other studies.

IV. SCATTERING FORMALISM

To compute the elastic scattering properties of dark atoms, we solve the Schrödinger equations for the partial wave radial functions $u_{\ell}^{s,t} = r\psi_{\ell}^{s,t}$:

$$\left(\partial_r^2 - \frac{\ell(\ell+1)}{r^2} + f(R, \alpha)(E - V_{s,t}) \right) u_{\ell}^{s,t}(r) = 0, \quad (2)$$

where ℓ is the relative orbital angular momentum of the atoms; r , E , and $V_{s,t}$ are in atomic units; and

$$f(R, \alpha) = m_{\mathbf{H}}\epsilon_0 a_0^2 = R + 2 + R^{-1} - \frac{1}{2}\alpha^2 \quad (3)$$

is the ratio of the $m_{\mathbf{H}}$ to $\mu_{\mathbf{H}}$. Here E is the total c.m. energy of the colliding \mathbf{H} atoms, and in the following we will ignore the binding energy (α^2) contribution to f to approximate it as a function only of R . It will be useful to note that the wave number in atomic units is given by $k = \sqrt{fE}$.

At distances large compared to the range of the potential, $u_{\ell}^{s,t}$ takes the asymptotic form proportional to $\sin(kr - \ell\pi/2 + \delta_{\ell}^{s,t}(k))$, where $\delta_{\ell}^{s,t}$ is the phase shift. The usual relation between the partial wave contribution to the cross section and the phase shift is $\sigma_{\ell} = (4\pi/k^2)(2\ell+1)\sin^2(\delta_{\ell}^{s,t})$, but in the present case we must take into account the multiplicity of the total nuclear spin, which is correlated to that of the electrons, since the total wave function must be symmetric under simultaneous interchange of both the electrons and the protons. Naively, this would give extra relative weights of $(1/16, 3/16)$ to the even- and odd- ℓ waves, respectively, of the singlet state (since the nuclei must have total spin 0 or 1,

respectively), while these weights would be $(9/16, 3/16)$ for the triplet. However, it has been shown [22] that indistinguishability of the two \mathbf{H} atoms gives rise to an additional factor of 2. Then the expression for the total unpolarized cross section is

$$\sigma = \frac{\pi}{2k^2} \sum_{\ell} (2\ell + 1) \begin{cases} \sin^2 \delta_{\ell}^s + 9\sin^2 \delta_{\ell}^t, & \ell \text{ even} \\ 3\sin^2 \delta_{\ell}^s + 3\sin^2 \delta_{\ell}^t, & \ell \text{ odd} \end{cases} \quad (4)$$

To extract the phase shifts, one integrates the Schrödinger equation from $r = \epsilon$ with $\epsilon \ll 1$ and $u_{\ell}(\epsilon) = 0$ out to some sufficiently large r where the u_{ℓ} is well approximated by the general $V = 0$ solution, $u_{\ell}(r) = C_1 j_{\ell}(kr) + C_2 n_{\ell}(kr)$. These are Riccati-Bessel functions, related to the corresponding spherical Bessel functions by a factor of r , so that their asymptotic behavior is $j_{\ell} \sim \sin(kr - \pi\ell/2)$, $n_{\ell} \sim -\cos(kr - \pi\ell/2)$. At sufficiently large r , the coefficients are given by

$$\begin{aligned} C_1 &= -n'_{\ell}(kr)u_{\ell}(r) + n_{\ell}(kr)u'_{\ell}(r)/k, \\ C_2 &= j'_{\ell}(kr)u_{\ell}(r) - j_{\ell}(kr)u'_{\ell}(r)/k, \end{aligned} \quad (5)$$

where k comes from the Wronskian, $j'_{\ell} = dj_{\ell}/d(kr)$, and the phase shift is then given by $\delta_{\ell} = \tan^{-1}(C_2/C_1)$. One can test for convergence by verifying that δ_{ℓ} is independent of r . We find that $r = 100$ is sufficient for energies up to $E = 0.1$ and $R < 10^4$.

V. ATOMIC SCATTERING LENGTHS

In the limit $E \rightarrow 0$, the s-wave contributions to the cross section approach constant values characterized by the scattering lengths

$$a_{s,t} = -\lim_{k \rightarrow 0} k^{-1} \tan \delta_0^{s,t}(k). \quad (6)$$

It can be calculated directly at $E = 0$ by a simpler method than that described for the phase shifts, since at $E = 0$ the

solution in the region outside the potential is linear, $u_0 = C_2 - C_1 r$. The scattering length is the value of r where this line intercepts the r axis: $a = C_2/C_1 = \lim_{r \rightarrow \infty} [-u_0(r)/u'_0(r) + r]$. Again we find $r \sim 100$ adequate for our purposes.

We first consider the proton-electron mass ratio $R = 1836.15$ that corresponds to the visible world. We find scattering lengths $a_s = 0.28$ and $a_t = 1.37$. These are in reasonable agreement with values found by other authors; for example, determinations of a_t in the atomic physics literature range from 1.2 to 2 [23]. Our values agree with those of Ref. [24]. By changing R from 1836 to 1835, we can also reproduce the incorrect value $a_s \cong 0.45$ obtained by several authors who neglected the electron mass contribution to $m_{\mathbf{H}}$ in Eq. (3), as has been discussed in Ref. [25].

We next explore the dependence of the scattering lengths on the proton-to-electron mass ratio R . The results are shown in Fig. 2. The triplet scattering length a_t varies relatively slowly with R , while the singlet one displays a large number of poles and zeroes in the interval $R \in [1, 5000]$. This number is directly related to the number of bound states supported by the corresponding potential. The dependence on R can be understood qualitatively from Eq. (2), which shows that the potential effectively becomes deeper as $f(R)$ increases. A semiclassical analysis indicates that the number of bound states should be of order $n \sim \pi^{-1} \int_{r_1}^{\infty} \sqrt{f(R)V} dr$, where r_1 is the $E = 0$ turning point; thus, we expect that the n th pole of a_s should occur at $R_n \sim n^2$. A numerical fit to the positions of the poles confirms this, giving $R_n \cong -3.45 + 9.49n + 7.74n^2$. The extreme shallowness of the triplet potential is such that the first bound state (first pole) only appears for $R > 2000$.

Figure 2 shows a close-up of the region around $R \sim 1836$ corresponding to normal atoms. It is a coincidence of nature that we fall so close to a zero of a_s , so that the triplet channel dominates even more than the 9:1 ratio of coefficients in Eq. (4) would imply. We will see below

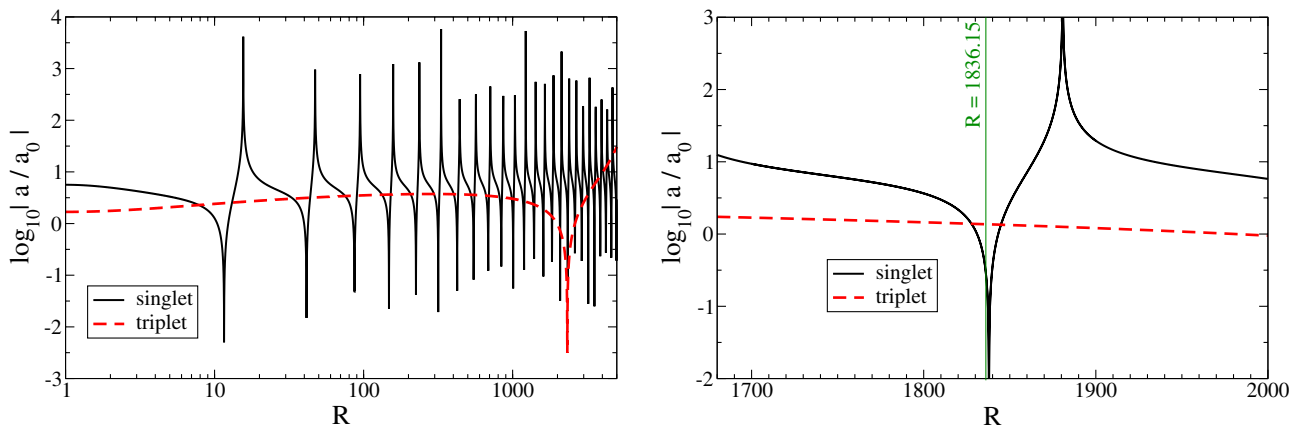


FIG. 2 (color online). Singlet and triplet scattering lengths as a function of $R \equiv m_{\mathbf{p}}/m_e$. The rightmost figure zooms in on the region around $R = 1836.15$, denoted by the vertical line.

that as a result of this accident, $R \sim 1836$ is close to a local minimum in the total cross section at low energy, considered as a function of R .

VI. ATOMIC CROSS SECTIONS

We now turn to the energy-dependent cross sections, exploring how they change with R . Our focus will be on low energies $E \lesssim 10^{-2}\epsilon_0$, for which the cross sections converge with the addition of a relatively small number of partial waves. At higher energies, convergence can require including terms with ℓ in the hundreds. For illustration and for comparison with previous results in the literature, we start with the real-world value of $R = 1836.15$. The result is shown in Fig. 3 for several different choices of the maximum partial wave number ℓ_{\max} . For energies up to $E = 10^{-3}$, $\ell_{\max} = 10$ is sufficient. For accurate predictions at $E = 10^{-2}$, up to 40 partial waves are required at $R = 1836$. (At smaller R , we observe that $\ell_{\max} = 10$ is sufficient for all energies below $E = 10^{-2}$.)

Figure 3 also plots previous results for atomic H scattering from Refs. [26–28]. The results are in reasonable agreement; in particular, the intricate structures we obtain at energies $E > 2 \times 10^{-4}$ match those of Ref. [28] (dotted curve) very well. The features can be understood on general physical grounds. Unlike molecular bond lengths and binding energies, which are expected to be determined by the atomic units rather than R , the scattering cross section is sensitive to the relation between energy and the de Broglie wavelength of the atom, which involves the atomic, rather than electronic, mass, and hence introduces R dependence.

Therefore, besides the energy scale ϵ_0 that defines the atomic unit of energy, there is a scale, $\epsilon_1 = \epsilon_0 R^{-1}$, where the incoming atom's de Broglie wavelength is of order a_0 and scattering becomes sensitive to the internal structure of the atom, and another, $\epsilon_2 = \epsilon_0 R^{-3/2}$, where the Van der Waals potential at a separation of one de Broglie

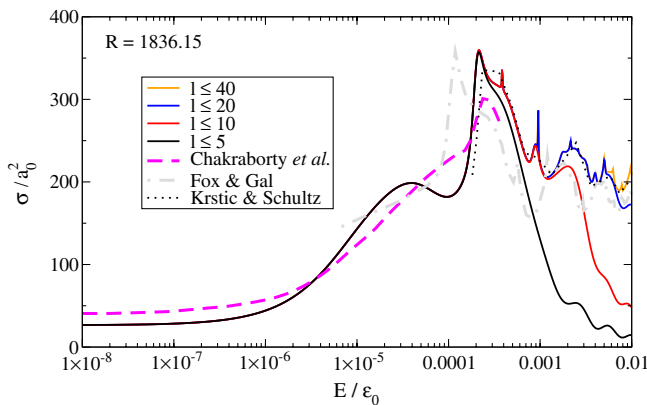


FIG. 3 (color online). Solid lines: Our results for the cross section with $R = 1836.15$ including partial waves up to $\ell = 5, 10, 20, 40$. Other curves: Previous results from Refs. [26–28].

wavelength is of the order of the kinetic energy. It is the energy scale ϵ_2 where scattering starts to change from being purely s wave to containing important contributions from higher partial waves. In Fig. 3, the cross section makes a transition from flat to rising behavior at $E \sim 10^{-5} \sim \epsilon_2$, and it starts falling again, while displaying numerous bumps and peaks, around $E \sim 10^{-3} \sim \epsilon_1$.

For general values of R , we find significant variations in the functional forms of $\sigma(E)$. Figure 4 gives a series of examples covering the ranges $R \in [15.5, 47]$ and $[1646, 1876]$ that span neighboring poles of a_s for representative cases of lower and higher R . Although generically the cross section approaches a constant as $E \rightarrow 0$, determined by the scattering lengths, $\sigma \rightarrow (\pi/2)(a_s^2 + 9a_t^2)$, if a_s diverges, then $\sigma \sim 1/k^2$. For values of a_s close to a pole, the transition between $\sigma \sim \text{constant}$ and $1/E$ behavior occurs at smaller energies than in the generic case. This can be seen in the graphs of Fig. 4 corresponding to $R = 15.5, 47, 1646$, and 1876 .

A more generic behavior is illustrated by the plots corresponding to $R = 18, 36, 43, 1670, 1750, 1802$; namely, σ remains close to its asymptotic $E = 0$ value until the scale ϵ_2 and then starts rising or falling, before entering the regime at ϵ_1 where rapid oscillations predominate with a slowly falling envelope. Whether σ falls or rises at $E = \epsilon_2$ depends on whether R is closer to being at a pole or a zero of a_s .

Various resonances appear as R is varied, but a particular one in the $\ell = 1$ singlet channel stands out, as is evident near $R = 25$ and 1685 . It becomes more prominent and narrow as R is increased up to some critical value, at which point it abruptly disappears. This can be understood as the energy of the resonance passing through zero at the critical value, after which it would only be seen for imaginary values of the wave number, that of course we do not consider. We expect the resonance energies to decrease with R , since increasing R makes the potential deeper [see Eq. (2)], causing all the energy levels to go down. This is also true for the positive-energy virtual states, which become negative-energy bound states as R increases.

The global behavior of $\sigma(E)$ as a function of R can also be visualized by plotting σ versus R at a few fixed energies. We show this for energies $E = 10^{-3}, 10^{-4}, 10^{-6},$ and $10^{-8}\epsilon_0$ in Fig. 5. Generally, we observe a minimum cross section of order $\sigma \sim 100a_0^2$, except in the region $R \sim 2000$ – 3000 near the first zero of the triplet scattering length. Curiously, the natural value $R = 1836$ is at a local minimum of the total cross section, as can be seen in the inset of the figure. Only three other zeroes of a_s correspond to such a low value of σ .

VII. DARK ATOM CONSTRAINTS FROM GALACTIC STRUCTURE

Self-interactions of dark matter have been studied in connection with their effects on structure formation within

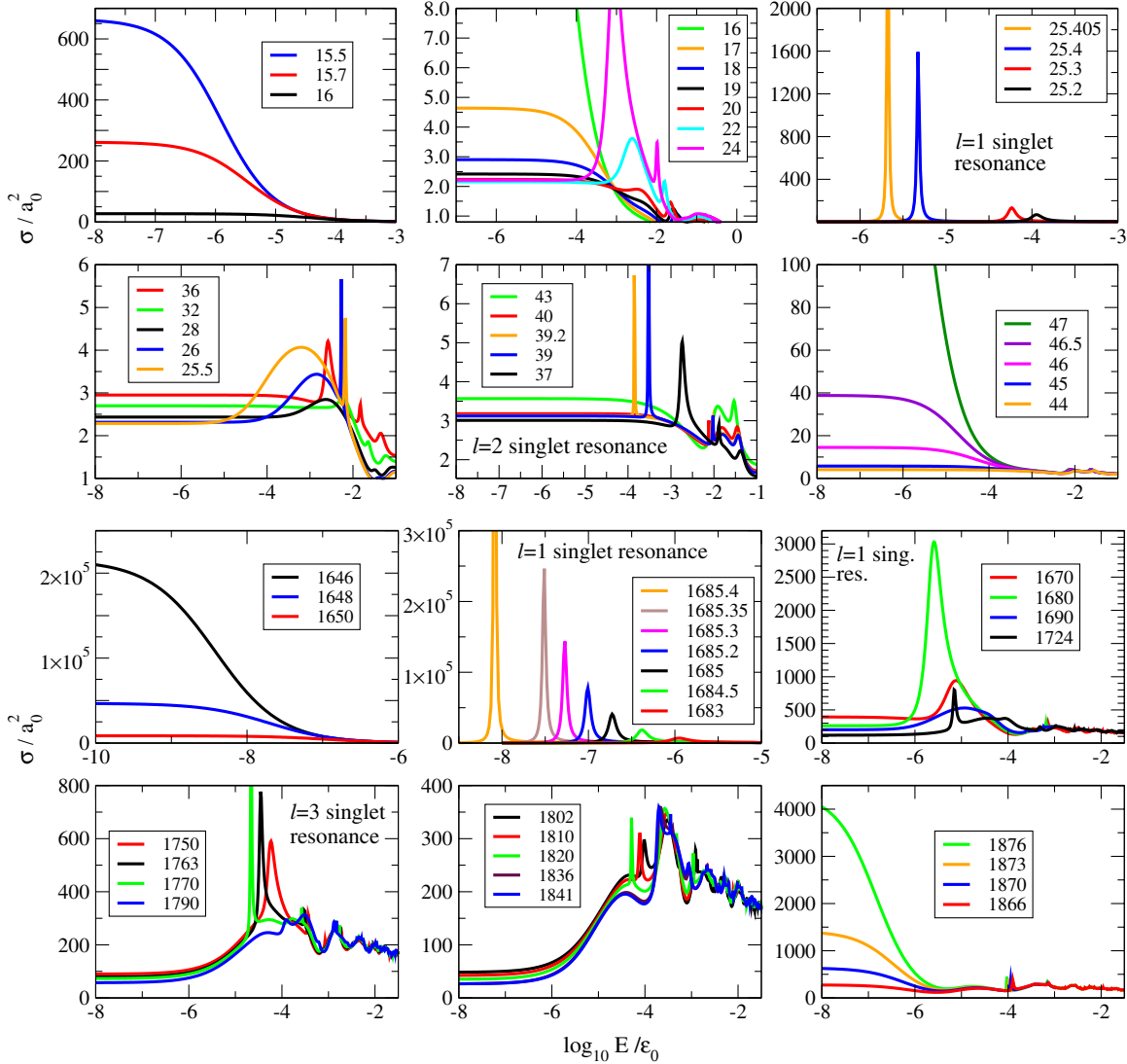


FIG. 4 (color online). Cross section as a function of energy for different values of R , which are indicated in the legends. For gray-scale viewers, the order of curves in the legends corresponds to that of the low-energy parts of the curves, from top to bottom.

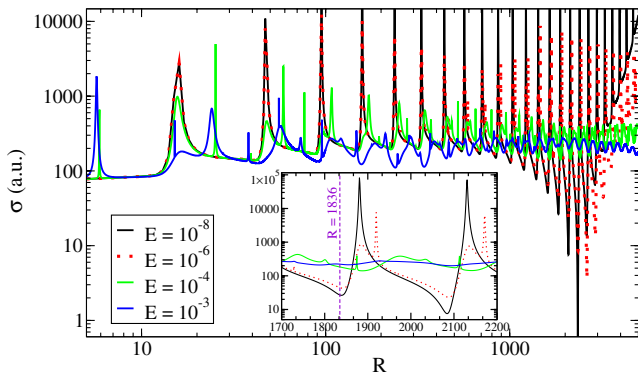


FIG. 5 (color online). Cross section as a function of R for different fixed values of the energy, $E = 10^{-3}$, 10^{-4} , 10^{-6} , and 10^{-8} in atomic units. (Lower energies generally correspond to larger σ .) The inset zooms in on the region near $R = 1836$.

galaxies and galactic clusters, leading to upper bounds on the cross section. The constraints come about because dark matter tends to be slower in the periphery of a bound structure, and the interactions between particles with large- and small-radius orbits can heat up the interior particles, causing them to escape to wider regions and leading to cored profiles for galaxies. On larger scales, the observed ellipticity of halos in clusters will be erased by strong self-scattering, leading to spherical halos.

Formerly, halo ellipticity was believed to give the strongest bound, $\sigma/m < 0.02 \text{ cm}^2/\text{g}$ [29] for DM with velocities of order 1000 km/s, characteristic of galactic clusters. But recent studies based upon N -body simulations [30] have concluded that the true bound is much weaker, at least as large as $0.1 \text{ cm}^2/\text{g}$, but smaller than $1 \text{ cm}^2/\text{g}$ [30]. The latter is consistent with similar bounds obtained from the Bullet Cluster [31,32] and from accretion of dark matter

by supermassive black holes in galactic centers [33]. (Reference [34] obtains a stronger constraint, which, however, depends upon assuming a cuspy profile for the DM halo, which might be erased by the self-interactions themselves.) Reference [35] constrains $\sigma/m < 0.4 \text{ cm}^2/\text{g}$ by requiring that elliptical galaxy halos within clusters not evaporate within 10^{10} yr at DM velocities of $v \sim 100\text{--}1000$ km/s, while Ref. [36] obtains $\sigma/m < 0.2 \text{ cm}^2/\text{g}$ from the inferred DM profile of a particular low-surface-brightness galaxy with $v \sim 150$ km/s, with input from then-current cosmological simulations. More recently, it has been argued [37] that a value of $\sigma \sim 0.6 \text{ cm}^2/\text{g}$ would be consistent with observed central densities of the Milky Way dwarf spheroidals at $v \sim 10$ km/s. Taking into account the probable though unspecified astrophysical uncertainties in these bounds, a reasonable and simple compromise would seem to be $\sigma/m < 0.5 \text{ cm}^2/\text{g}$ [38], which we adopt in the following. We will apply this bound over the range of velocity scales $v \in [10, 1000]$ km/s that are relevant for dwarf spheroidals up to galactic clusters in the following.

Scatterings in the forward direction are not effective for exchanging energy between dark matter particles, which is the basis for the constraints on σ . Therefore, the bound should be applied not to the elastic cross section σ_{el} , but rather to the transport cross section σ_t , which gives a better representation of scatterings that involve significant exchange of momentum. A commonly used expression for the transport cross section is $\sigma_t = 2\pi \int d(\cos\theta)(1 - \cos\theta)d\sigma/d\Omega$. But this expression is not appropriate for scattering between identical particles, since backward scattering is indistinguishable from forward scattering and is also not effective at modifying the momentum distribution. Therefore, it is more appropriate to use $\sigma'_t = 2\pi \int d(\cos\theta)(1 - \cos^2\theta)d\sigma/d\Omega$, which treats forward and backward scattering as equivalent.¹ In terms of partial waves, it is given by [39]

$$\sigma'_t = \frac{6\pi}{k^2} \sum_{\ell} \frac{(\ell+1)(\ell+2)}{(2\ell+3)} \sin^2(\delta_{\ell} - \delta_{\ell+2}) \quad (7)$$

for a generic scattering problem. For the current application, Eq. (4) is adapted by replacing $(2\ell+1)$ with $(3/2)(\ell+1)(\ell+2)/(2\ell+3)$ and δ_{ℓ} by $\delta_{\ell} - \delta_{\ell+2}$. The normalization is such that at low energies where only the s wave contributes, $\sigma'_t = \sigma_{\text{el}}$.

To illustrate the difference between the elastic and transport cross sections, we plot σ_{el} and σ'_t for a few

¹Here we disagree with Refs. [15] and [28], which use σ_t and therefore find that the elastic and transport cross sections are equal for identical particles. Their approach is based on treating forward scattering as irrelevant [$1 - \cos(\theta) = 0$] but backward scattering as of maximal relevance [$1 - \cos(\theta) = 2$], which is inconsistent, since for identical particles these processes are equivalent.

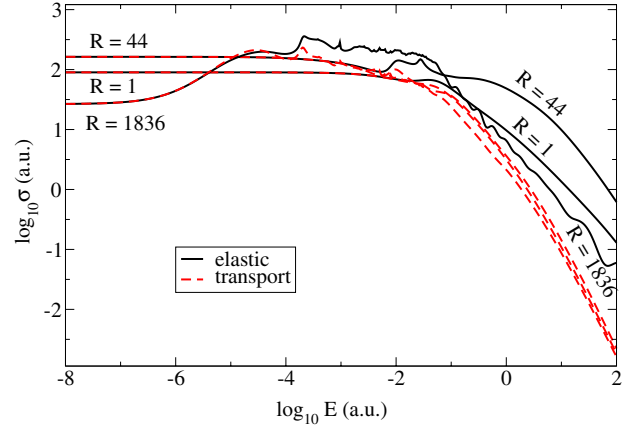


FIG. 6 (color online). Elastic (solid lines) and transport (dashed) dark atom cross sections versus energy for $R = 1, 44,$ and 1836.15 .

representative values of R in Fig. 6. As expected, at low energy, where s -wave scattering dominates, the two are equal, but they differ at energies $E \gtrsim 0.1\epsilon_0$, where higher partial waves become important. We find that $\sigma'_t \propto 1/E$ for $0.1\epsilon_0 < E < \epsilon_0$ and $\sigma'_t \propto 1/E^2$ at higher energies. (See the next section for a more detailed quantification of this dependence.) We use this scaling in what follows in order to speed up computations of σ'_t above $0.1\epsilon_0$, since the addition of many partial waves is time consuming. The asymptotic behavior $\sigma'_t \propto 1/E^2$ is expected, since at high energies the scattering is dominated by screened Coulomb scattering of the dark protons, which shows exactly this energy dependence (up to logs). We therefore expect this scaling to be valid also for inelastic contributions to the cross sections (such as from electronic transitions) that are energetically allowed for $E > \epsilon_0$. We disagree with the assumption in Ref. [15] that the cross sections drop exponentially with E for $E > \epsilon_0$, which contradicts our expectations based on Coulomb scattering.

To constrain the parameter space of atomic DM, we impose the bound $\sigma'_t < 0.5 \text{ cm}^2/\text{g}$ at several different DM velocities, $v = 10, 30, 100, 300, 1000$ km/s, using $E = f(R)(v/c\alpha)^2\epsilon_0$. We scan the R - m_{H} plane for a range of α to find upper limits on m_{H} as a function of R . The results are shown in Fig. 7(a). The constraints show nonmonotonic dependence on α , which we can understand as follows: For very small α , the binding energy is small, so the kinetic energy is large compared to the binding energy. In this regime the scatterings are essentially Coulomb scatterings between the dark protons, and smaller α leads to less scattering. But as α is increased, the binding energy becomes larger than the kinetic energy, and the scatterings really involve the whole atoms. Now, larger α means more tightly bound and therefore smaller atoms, hence a decreasing cross section with increasing α . Alternatively, one could say that for small α , the formation of atoms fails to screen the Coulomb interaction, so scattering rates scale as

expected with coupling strength. But as the coupling increases, the charges are ever more effectively screened within atoms, and the residual interactions get weaker with increasing α .

In terms of dependence upon R , we expect these results to be accurate for $R \gg 1$ where the Born-Oppenheimer approximation holds. Then the scattering potentials are essentially independent of R when expressed in atomic units, as we have assumed. This need no longer be the case when $R \sim 1$.

However, we have unrealistically assumed up until now that there is no significant fraction of dark ions. In Ref. [10], the ionization fraction f_i was numerically determined over a range of parameters. We find that a good fit to their results is given by the simple estimate

$$f_i \cong \min [10^{-10} \xi \alpha^{-4} R^{-1} (m_{\mathbf{H}}/\text{GeV})^2, 1], \quad (8)$$

where $\xi = T_d/T_\gamma$, the present ratio of the dark to the visible photon temperatures, which was taken to be 1 in Ref. [10]. This agrees with the result derived by Ref. [15], which takes $\xi = 0.4$, while noting that the uncertainty in the estimate [Eq. (8)] is greater than the difference made by including the factor of ξ , which we take to be 1 in the following.² It is then straightforward to show that the region of the R - $m_{\mathbf{H}}$ plane covered by Fig. 7 corresponds to $f_i \sim 0$ for $\alpha > 0.05$, while for $\alpha < 10^{-3}$, $f_i \sim 1$ over the entire region. The boundaries above which f_i becomes ~ 1 are shown as diagonal lines for the transition values $\alpha = 0.01, 0.02, 0.03$ in Fig. 7(b). Hence, we can ignore the effect of ionization on our constraints for $\alpha \gtrsim 0.03$, but it becomes important at slightly lower values. The transition is rather sudden due to the high power of $1/\alpha$ in Eq. (8).

Reference [40] has considered the constraints from halo ellipticity and from the Bullet Cluster on fully ionized atomic dark matter, numerically finding the former to give a much stronger constraint, which we fit to the form

$$\frac{m_{\mathbf{H}}}{\text{GeV}} > (10^{6.7} \alpha)^{2/3}. \quad (9)$$

Rather than computing a cross section and comparing it to a limiting value, which is valid in the approximation that the scattering potential can be modeled as a hard sphere (the assumption used in deriving the limiting cross sections), Ref. [40] compares the time needed to have several hard scatterings to the dynamical time scale for the cluster as the

²In principle, ξ is a free parameter that is only determined by the relative efficiency of reheating in the dark and visible sectors after inflation, unless there are significant interactions between the two sectors that we do not consider in this work. Generically, one would expect that $\xi \sim 1$ unless there is some (model-dependent) reason for reheating only to the visible sector. Reference [15] shows that big bang nucleosynthesis bounds $\xi < 0.83$ – 0.9 at 3σ , depending upon the number of relativistic dark species at the time.

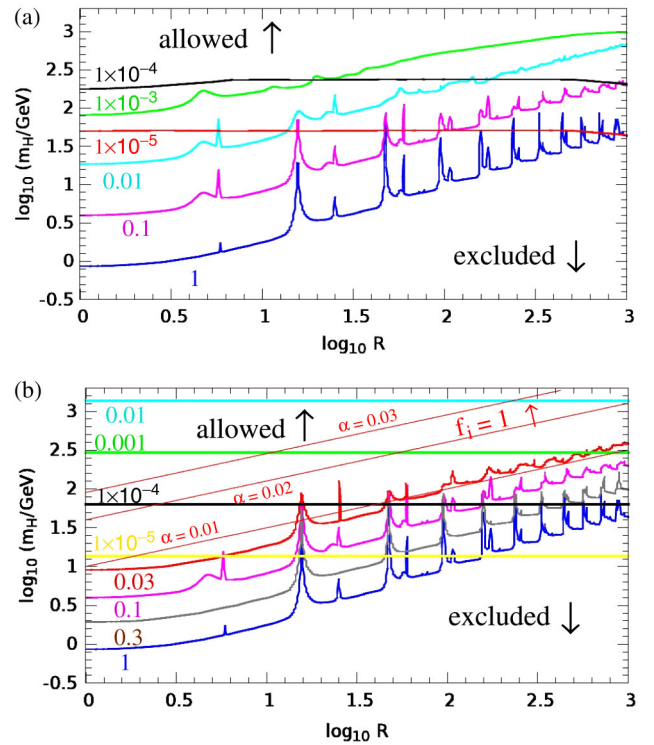


FIG. 7 (color online). (a) Uppermost: Lower limit on the dark atom mass as a function of R , from halo constraints on dark matter self-interactions, assuming no ionization. The curves are labeled by the value of $\alpha = 1, 0.1, \dots, 10^{-5}$, which is held fixed. (b) Lower: Modified limits, taking into account the ionized fraction of dark atoms. Thin diagonal lines indicate the boundary above for which the ionization fraction is ~ 1 for $\alpha = 0.01, 0.02$ and 0.03 , according to Eq. (8) with $\xi = 1$.

criterion for erasure of ellipticity. The Coulomb cross section is infrared divergent due to soft scatterings, and even the momentum-transfer cross section has a logarithmic remnant of this divergence that gets cut off by the Debye screening length of the DM plasma; hence the need for a specialized treatment.

The bounds we obtained for $\alpha < 0.1$ in Fig. 7(a) are thus superseded by Eq. (9), indicated by the horizontal lines in the amended Fig. 7(b), which also shows the elastic scattering bound for the additional values of $\alpha = 0.3, 0.03$. These bounds are quite sensitive to the assumed value of the lowest velocity at which the constraints are applicable, since they are determined by the region of energies where $\sigma'_i \propto 1/E^2$. They should thus be considered as approximate, requiring a more detailed study of the effect of such a strongly velocity-dependent cross section on dwarf galaxies, where $v \sim 10$ km/s applies.

We also plot our constraints in the $m_{\mathbf{H}}$ - α plane for a few fixed values of the dark atom binding energy in Fig. 8, for comparison with Ref. [15] which presents its results in this way. The parts of the constraints coming from the fully ionized versus the fully atomic forms are marked on the figure. We have computed the ionization fraction using

Eq. (8), assuming $\xi = 0.37$ as in Ref. [15]. Because it is numerically difficult for us to compute the cross section for $R > 10^4$, we do not consider these regions (so labeled) in the upper-right corners. The lower-left corners are physically inaccessible, since the binding energy is given by $B_H = \frac{1}{2}\alpha^2 m_H / f(R)$, and $f(R) \equiv R + 2 + 1/R$ cannot be less than 4. As in Fig. 7(b), we approximate the transition between ionized and atomic DM as sudden, which explains the sharpness of the curves in the vicinity of $m_H = 10^{3-3.5}$ in the lower two graphs of Fig. 8. (We expect the ion constraints to disappear for $f_i \lesssim 0.5$, since in that case the halo ellipticity within the large atomic fraction remains

relatively undisturbed.) In these regions the constraint is coming from the fully ionized constituents. On the other hand, the jaggedness of the constraint in the upper-left corner of the $B_H = 10$ MeV graph is a direct reflection of the strong R dependence of the atomic scattering cross section, which was not taken into account in Ref. [15]. We find that the allowed regions are generally larger than given in that work.

VIII. ANALYTIC FITS TO TRANSPORT CROSS SECTION

As is apparent from Fig. 4, it would be difficult to give analytic formulas for the energy dependence of the atomic scattering cross sections in the cases where there are strong resonances or vanishing scattering lengths. On the other hand, there are many examples, such as the cases $R = 1$ and 44 shown in Fig. 6, where σ'_i has a rather simple dependence, which we find can be satisfactorily fit by the *Ansatz*

$$\sigma'_i \cong (a_0 + a_1 E + a_2 E^2)^{-1}, \quad (10)$$

TABLE I. Coefficients of the *Ansatz* [Eq. (10)] that give the best fit to the transport cross section for the given value of R . The quality of the fit is indicated by χ^2 .

R	a_0	a_1	a_2	χ^2
1	0.011	0.221	0.063	0.084
5	0.011	0.178	0.060	1.696
10	0.012	0.197	0.053	0.056
20	0.006	0.251	0.045	0.288
30	0.007	0.241	0.044	0.208
40	0.008	0.233	0.044	0.194
50	0.003	0.331	0.038	2.599
60	0.005	0.277	0.041	1.026
70	0.006	0.259	0.043	0.567
80	0.006	0.251	0.043	0.412
90	0.006	0.258	0.043	0.631
100	0.003	0.325	0.039	2.726
200	0.005	0.280	0.045	0.942
300	0.005	0.281	0.047	0.972
400	0.005	0.290	0.049	1.000
500	0.005	0.306	0.051	1.157
600	0.004	0.333	0.051	2.065
700	0.005	0.333	0.053	2.120
800	0.006	0.320	0.056	0.876
900	0.004	0.364	0.055	2.208
1000	0.007	0.318	0.060	0.593
1500	0.006	0.398	0.062	1.351
2000	0.008	0.407	0.069	2.964
2500	0.008	0.472	0.070	2.272
3000	0.003	0.697	0.062	4.531
3500	0.005	0.647	0.070	3.677
4000	0.002	0.970	0.059	10.014
4500	0.002	1.045	0.060	15.530

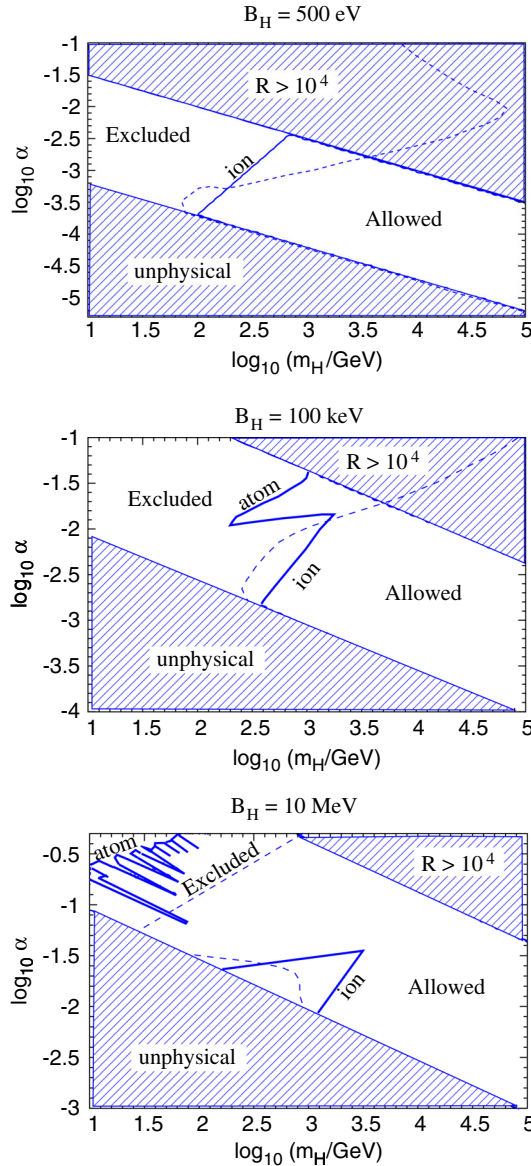


FIG. 8 (color online). The solid curves give the boundaries between the allowed and excluded regions of atomic DM parameter space for fixed values of the binding energy, $B_H = 500$ eV, 100 keV, 10 MeV, for comparison with Fig. 20 of Ref. [15], whose constraints are given by the dashed curves.

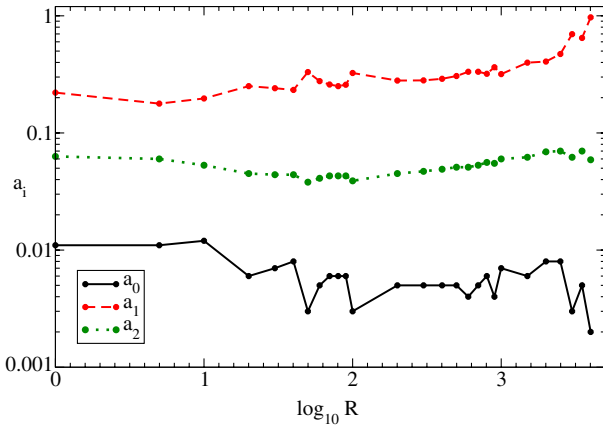


FIG. 9 (color online). Graphical representation of R dependence of the fit coefficients given in Table I.

where all quantities are expressed in atomic units. We focus here on the transfer cross section rather than the elastic one, since it is the more physically relevant quantity for applications such as those considered in the previous section. In Table I, we give the best-fit values of the coefficients a_i for the transport cross section for a selection of R values. The goodness of the fit is also given there as

$$\chi^2 = \sum_{i=1}^{101} \log_{10}^2(\sigma'_i/\text{fit}), \quad (11)$$

where the sum is over 101 uniformly spaced values of $\log_{10}(E) \in [-8, 2]$. We plot the coefficients a_i versus R in

Fig. 9 to underscore that they tend to vary rather slowly with R , especially a_1 , which determines the behavior at intermediate energies.

The fits are graphically compared to the accurate cross sections in Fig. 10. On a log scale they all look rather good, but the errors can be significant for examples with $\chi^2 \gtrsim 1$. For example, at $R = 100$ with $\chi^2 = 1$, the maximum error is a factor-of-2 discrepancy at $E = 10^{-2.5}$. As R increases, the accuracy tends to get worse. At $R = 4000$, the fit is 4 times greater than the actual cross section at $E = 10^{-4}$. For $R = 1$, on the other hand, the maximum error is only 20%. Unless one happens to choose a value of R that gives a large resonance or a zero of the singlet channel scattering length, a reasonable approximation to the transfer cross section can be obtained by interpolating the above results. For example, at $R = 15.5$, where there is such a zero (see Fig. 4), we find $\chi^2 = 130$, and the fit underestimates the actual σ'_i by 2 orders of magnitude at low energies (although it still does well for $E \gtrsim 10^{-4}$). In the case of a large resonance as in $R = 25.405$, we find $\chi^2 = 7.9$, with the error coming from energies at and below the resonance region, while the fit remains good for $E > 10^{-5}$.

IX. DARK MOLECULAR H_2 ABUNDANCE

So far, we have assumed that dark atoms do not predominantly combine to form the analog of H_2 molecules. In the cosmos, the proportion of real H_2 molecules is small, because the molecular binding energy 4.5 eV is less than the energy of Ly- α photons that were copiously produced by young, massive, hot stars. H_2 is thus easily

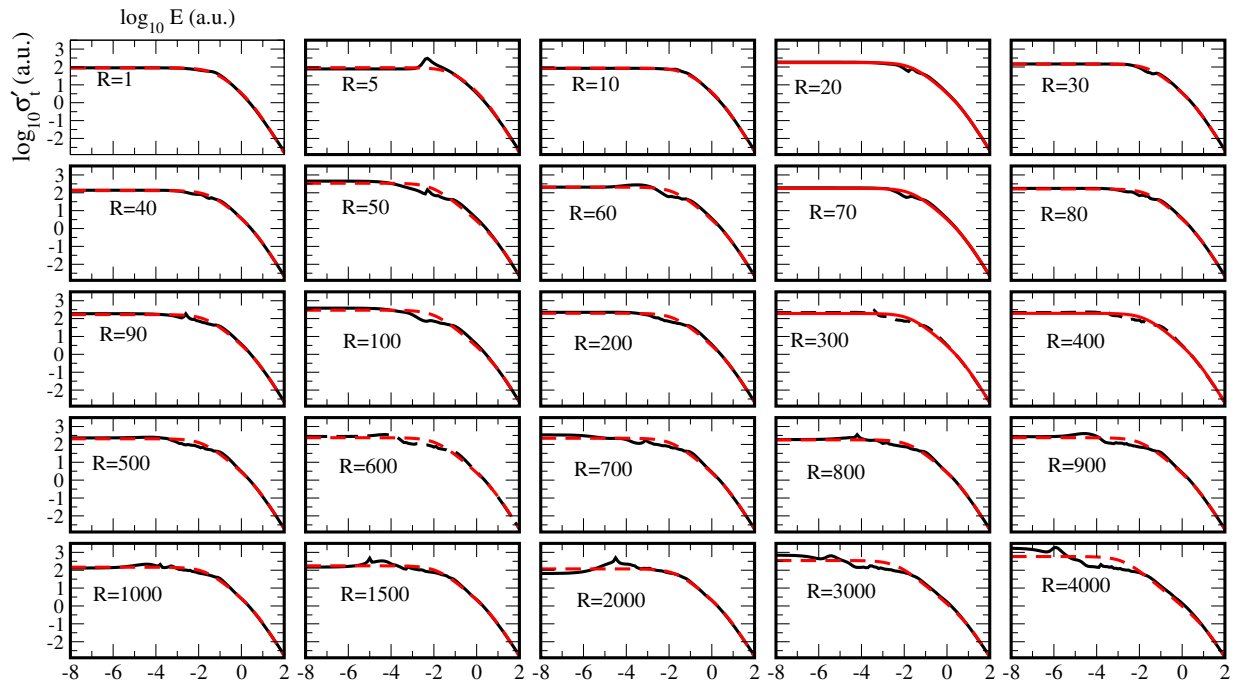


FIG. 10 (color online). Comparison of atomic momentum-transfer cross section (solid lines) with the best fit using the *Ansatz* [Eq. (10)] (dashed) for a range of R values. Here $\log_{10}\sigma'_t$ versus $\log_{10}E$ is plotted, in atomic units.

dissociated by a readily available form of radiation. On the other hand, it is slow to form because it has no electric dipole moment, and the reaction $\text{H} + \text{H} \rightarrow \text{H}_2 + \gamma$ proceeds through an electric quadrupole transition, occurring only once in every 10^5 scatterings. Much more efficient means of producing H_2 are the catalyzed reactions ($\text{H} + p \rightarrow \text{H}_2^+$, $\text{H}_2^+ + \text{H} \rightarrow \text{H}_2 + p$) and ($\text{H} + \text{H}^- \rightarrow \text{H}_2^-$, $\text{H}_2^- + \text{H} \rightarrow \text{H}_2 + \text{H}^-$) that rely upon a small ionized population.

In the dark universe, assuming no analog of weak interactions, there will be no dark stars in the conventional sense that would produce ionizing dark radiation. Any stars that form from dark matter will be powered only by gravitational contraction as the protostellar cloud slowly cools and pressure rises. There will generically still be some ionized fraction f_i of dark atoms, however, as given in Eq. (8) This creates the potential for H_2 to become the prevalent form of dark matter in such a scenario.

If R is large, the predomination of H_2 is undesirable, because the rotational excitations of H_2 have small energies, $E_r = \ell(\ell + 1)/2I$, where $I \sim m_{\text{H}} a_0^2$ is the moment of inertia. In atomic units, $E_r \sim \mu_{\text{H}}/m_{\text{H}} = 1/f(R)$. Collisions of H_2 molecules with kinetic energies greater than this can be inelastic, exciting the rotational states, which can decay via quadrupole radiation. The ensuing dissipation of the DM kinetic energy will allow its halo to collapse in the same way as luminous matter. A complete study of this issue is beyond the scope of this paper; for now we merely note that large values of R might turn out to be untenable.

This leaves open the question of how large the value of R must be to really be considered large in the context of inelastic H_2 scattering. Interestingly, we can make a quantitative estimate using the machinery of the previous sections. Because H_2 has no dipole moment, rotational or ro-vibrational transitions involve electric quadrupole radiation, which requires a bound state with $J \geq 2$. Therefore, rotational and ro-vibrational emission is only possible if there is at least one bound state in the $\ell = 2$ channel. By solving the Schrödinger equation (2) at $E = 0$ and $\ell = 2$, we can identify the lowest value of R for which a d -wave bound state (indicated by a node in its wave function) exists between two H atoms. It turns out to be at $R = 15.42$, close to the first pole of a_s . This value of R is large enough so that the Born-Oppenheimer approximation is still reasonable; hence, we can expect it to be a fairly good estimate of the value of R below which no low-energy rotational transitions are available, and the ground state H_2 molecule is safe from making dangerous inelastic transitions, even if it does dominate over dark atoms.

X. SCATTERING OF DARK H_2 MOLECULES

Given a potential energy for H_2 self-interactions, we can use the same methodology as for atoms to estimate the cross section for elastic H_2 scattering. A number of *ab initio* calculations of H_2 - H_2 potentials have been given in the

literature, as well as some phenomenological *Ansätze* that have been fit to physical properties, including the cross section. At energies $E \gtrsim 1/R$, the calculation is complicated by the fact that the potential depends upon the relative orientations of the two molecules. At low energies where the rotational states are not excited, one can use the spherically symmetric term in the potential. The Schrödinger equation for molecular scattering differs from Eq. (2) by the replacement $f \rightarrow 2f$ due to the mass of H_2 . Similarly, the wave number is given by $k = \sqrt{2fE}$ in atomic units. The elastic cross section for para- H_2 scattering is given by [41]

$$\sigma = \frac{8\pi}{k^2} \sum_{\text{even } \ell} (2\ell + 1) \sin^2(\delta_\ell), \quad (12)$$

with the extra factor of 2 coming from the symmetry of the scattering amplitude under $\theta \rightarrow \pi - \theta$ for identical particles, as we also had for atomic scattering.

It is possible to obtain a good description of experimentally measured cross sections for H_2 - H_2 scattering at low energies with a potential of the same form as Eq. (1), using for para- H_2 the parameter values $c_0 = 3.778$, $c_1 = 1.947$, $c_2 = 3.763 \times 10^{-3}$, $C_6 = 12.0$, $C_8 = 239.9$, $C_{10} = 0$ [41]. Reference [41] does not include the D factor, needed to keep the long-distance part of the potential from contributing as $r \rightarrow 0$, but we find that using $r_1 = 4$ gives satisfactory suppression without changing the behavior near the shallow minimum of the potential, at $r_m \sim 6.5a_0$ with $V_m \cong -10^{-4}\epsilon_0$. We plot the resulting cross section in Fig. 11, along with the result of Ref. [42] based upon an *ab initio* determination of the orientationally averaged potential. The results are in fair agreement, with a 10% discrepancy at low E , which is due to the difference between the large- r part of the Bauer *et al.* potential [41] we have adopted and that assumed in Ref. [42].

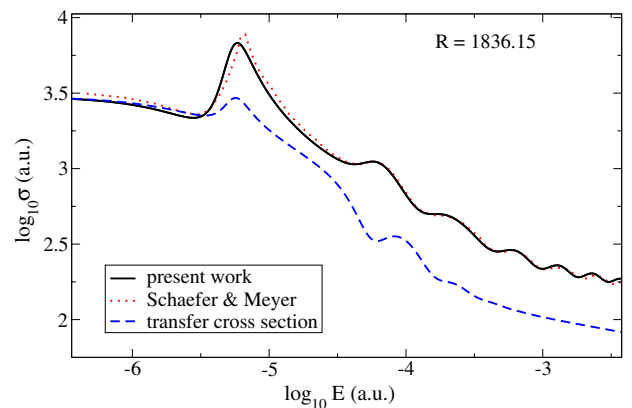


FIG. 11 (color online). Elastic scattering cross section of para- H_2 from *ab initio* calculation of Ref. [42] (dotted curve) and our own calculation based upon the potential of Ref. [41] (described in text). The dashed curve shows the momentum-transfer cross section (present work).

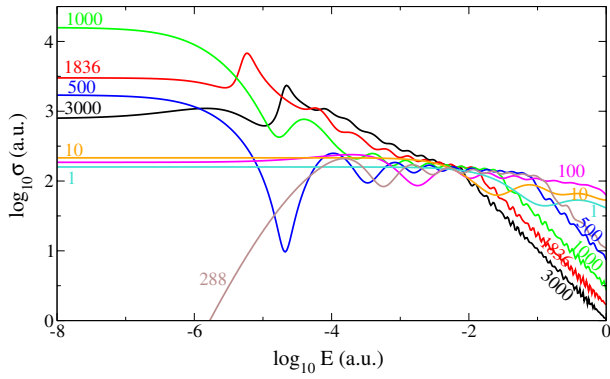


FIG. 12 (color online). Elastic cross sections for para- H_2 versus energy, for $R = 1, 10, 100, 288, 500, 1000, 1836,$ and 3000 .

Having reproduced known results at $R = 1836$, we explore the dependence of $\sigma(E)$ on R for dark molecules. A sample of cross sections for representative values of R is given in Fig. 12. Like for atoms, the cross sections generically approach a constant at low energies from the s -wave contribution, and they start to exhibit structure from the higher partial waves at energies $\epsilon_2 \sim R^{-3/2}\epsilon_0$. An exceptional case is shown for $R = 288$, close to the first zero of the scattering length, in which the constant behavior is delayed until smaller energies. A complementary view is given in Fig. 13, which plots σ at $E = 10^{-8}\epsilon_0$ as a function of R . Because the potential is quite shallow, there is only one bound state (giving a divergence of the scattering length when its energy vanishes) for $R < 4000$. The weakly bound state enhances the cross section for $R \sim 1000$, making it an order of magnitude or more larger than the typical value for dark atoms in this region of R .

Following the same procedure as for atomic dark matter, we have estimated the constraints from structure formation on the dark atom mass in the case where it is in molecular form. The momentum-transfer cross section is given again by replacing $(2\ell + 1) \rightarrow (3/2)(\ell + 1)(\ell + 2)/(2\ell + 3)$ and $\delta_\ell \rightarrow \delta_\ell - \delta_{\ell+2}$ in Eq. (12), the effect of which is

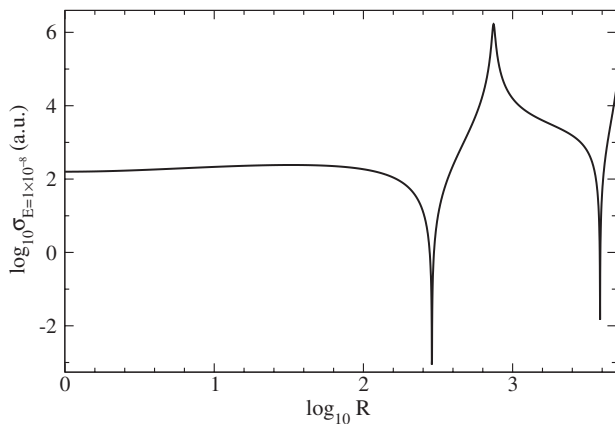


FIG. 13. Elastic cross section for para- H_2 versus R , at energy $E = 10^{-8}\epsilon_0$.

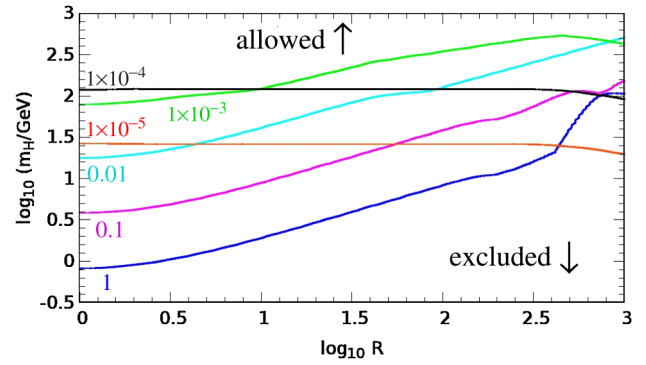


FIG. 14 (color online). Upper limits on m_{H} versus R from the halo structure for molecular dark matter, at $\alpha = 1, 0.1, \dots, 10^{-5}$. The mass plotted is still that of the atom, m_{H} .

indicated in Fig. 11. The resulting bounds, shown in Fig. 14, are rather similar to those we found for dark atoms in Fig. 7(a), except for the absence of sharp features, thanks to the relative smoothness of the molecular scattering length as a function of R (see Fig. 13). The bounds for molecular dark matter are stronger at $R \sim 1000$ and $\alpha \sim 1$ than for atomic DM because of the larger cross section at low energies. Like in the case of dark atoms, we expect the constraints for $\alpha \lesssim 10^{-2}$ to be stronger than shown here, since the ionization fraction is estimated to be large and the assumption of domination by the molecular state will not be correct. Nevertheless, we show them for comparison with Fig. 7(a). The constraints from the ionized fraction at small α will be the same as in Fig. 7(b).

In deriving these constraints, we have neglected the inelastic contributions from ro-vibrational transitions that become energetically allowed for $E \gtrsim R^{-1}$. Reference [43] shows that these are individually much smaller than the elastic cross section. For example, excitations from the ground state to the lowest rotational states have cross sections of ~ 9 a.u. at $E = 0.04\epsilon_0$, while transitions to the next lowest excitations have cross sections an order of magnitude smaller. At this energy, the elastic cross section is still 40 a.u. Thus, the elastic part may be a better estimate of the total cross section than one might have guessed.

XI. SUMMARY AND CONCLUSIONS

We have computed the cross sections for elastic scattering of dark atoms and molecules, whose properties are analogous to those of the visible world, and determined by the coupling strength α , the atom mass m_{H} , and the ratio R of dark proton and electron masses. In a world with $R = 1836.15$, and assuming $\alpha \ll 1$, there would be nothing to do, since the properties of dark atoms and molecules would be identical to those of their visible counterparts once expressed in the atomic units of length $a_0 = (\alpha\mu)^{-1}$ and energy $\epsilon_0 = \alpha^2\mu$. The nontrivial part of our job was to investigate how scattering changes as a function of R . Fortunately, for $R \gg 1$, the Born-Oppenheimer

approximation tells us that the interaction potentials (in atomic units) do not depend upon R . All the R dependence is kinematic and appears in the Schrödinger equation. By solving the Schrödinger equation using accurate determinations for the potentials, we are able to make quantitative predictions for dark atom scattering at $R \gg 1$.

We found that the cross sections for atom-atom scattering depend very strongly upon R , due to the number of bound states of the singlet scattering channel changing rapidly with R , with consequent divergences (and zeroes) in the singlet channel scattering length. The triplet channel has a shallower potential, and thus a less pronounced R dependence. The same is true for scattering of dark molecules, whose interaction potential is also shallow. Our exploration of the cosmology of dark molecules, though cursory, is the first one in the literature that we are aware of, and may lay useful groundwork for further study. One conclusion is that dark molecules may be disfavored for $R \gtrsim 15$, since in that case the inelastic scattering into rotationally excited states could make the DM too dissipative to remain in an extended halo.

As an application, we determined constraints from self-interactions on the atomic dark matter parameter space following from observations of halo ellipticity and central

densities of dwarf spheroidal galaxies. Moreover, we have given simple analytic fits to the energy dependence of the momentum-transfer cross sections that are accurate to 20% in some cases (despite the general complexity of the functions being modeled) and good enough for order-of-magnitude estimates in many other cases. These results improve upon previous ones in the literature by virtue of our more accurate cross sections, with respect to energy and R dependence, and by properly distinguishing between the elastic and momentum-transfer cross sections. In addition to constraints, there are suggestions that such self-interactions could be useful for addressing discrepancies between predictions of cold dark matter and some aspects of observed structure formation on small scales. One could thus anticipate that some of the borderline regions may actually be favored. We will address this issue in more detail in an upcoming paper.

ACKNOWLEDGMENTS

We thank Francis-Yan Cyr-Racine, Gil Holder, and Kris Sigurdson for helpful discussions or correspondence. J. C. thanks the Aspen Center for Physics for its congenial working environment while this research was in progress.

-
- [1] H. M. Hodges, *Phys. Rev. D* **47**, 456 (1993).
 - [2] H. Goldberg and L. J. Hall, *Phys. Lett. B* **174**, 151 (1986).
 - [3] Z. G. Berezhiani and R. N. Mohapatra, *Phys. Rev. D* **52**, 6607 (1995).
 - [4] Z. G. Berezhiani, A. D. Dolgov, and R. N. Mohapatra, *Phys. Lett. B* **375**, 26 (1996).
 - [5] R. Foot and R. R. Volkas, *Phys. Rev. D* **52**, 6595 (1995).
 - [6] R. N. Mohapatra and V. L. Teplitz, *Phys. Rev. D* **62**, 063506 (2000).
 - [7] R. Foot, *Int. J. Mod. Phys. D* **13**, 2161 (2004).
 - [8] M. J. Strassler and K. M. Zurek, *Phys. Lett. B* **651**, 374 (2007).
 - [9] N. Arkani-Hamed, D. P. Finkbeiner, T. R. Slatyer, and N. Weiner, *Phys. Rev. D* **79**, 015014 (2009).
 - [10] D. E. Kaplan, G. Z. Krnjaic, K. R. Rehermann, and C. M. Wells, *J. Cosmol. Astropart. Phys.* **05** (2010) 021.
 - [11] S. R. Behbahani, M. Jankowiak, T. Rube, and J. G. Wacker, *Adv. High Energy Phys.* **2011**, 709492 (2011).
 - [12] D. E. Kaplan, G. Z. Krnjaic, K. R. Rehermann, and C. M. Wells, *J. Cosmol. Astropart. Phys.* **10** (2011) 011.
 - [13] J. M. Cline, Z. Liu, and W. Xue, *Phys. Rev. D* **85**, 101302 (2012).
 - [14] J. M. Cline, Z. Liu, and W. Xue, *Phys. Rev. D* **87**, 015001 (2013).
 - [15] F.-Y. Cyr-Racine and K. Sigurdson, *Phys. Rev. D* **87**, 103515 (2013).
 - [16] F.-Y. Cyr-Racine, R. de Putter, A. Raccanelli, and K. Sigurdson, [arXiv:1310.3278](https://arxiv.org/abs/1310.3278).
 - [17] D. H. Weinberg, J. S. Bullock, F. Governato, R. K. de Naray, and A. H. G. Peter, [arXiv:1306.0913](https://arxiv.org/abs/1306.0913).
 - [18] W. Kolos and L. Wolniewicz, *Chem. Phys. Lett.* **24**, 457 (1974).
 - [19] I. F. Silvera, *Rev. Mod. Phys.* **52**, 393 (1980); I. F. Silvera and J. M. Walraven, *Prog. Low Temp. Phys.* **10**, 139 (1986).
 - [20] L. Wolniewicz, *J. Chem. Phys.* **99**, 1851 (1993).
 - [21] B. R. Joudeh, *Physica (Amsterdam)* **421B**, 41 (2013).
 - [22] M. J. Jamieson, A. Dalgarno, B. Zygelman, P. Krstić, and D. Schultz, *Phys. Rev. A* **61**, 014701 (1999).
 - [23] A. Sen, S. Chakraborty, and A. S. Ghosh, *Europhys. Lett.* **76**, 582 (2006).
 - [24] C. J. Williams and P. S. Julienne, *Phys. Rev. A* **47**, 1524 (1993).
 - [25] M. J. Jamieson and A. Dalgarno, *J. Phys. B* **31**, L219 (1998).
 - [26] S. Chakraborty, A. Sen, and A. S. Ghosh, *Eur. Phys. J. D* **45**, 261 (2007).
 - [27] J. W. Fox and E. Gal, *Proc. Phys. Soc. London* **90**, 55 (1967).
 - [28] P. Krstic and D. Schultz, *J. Phys. B* **32**, 3485 (1999).
 - [29] J. Miralda-Escude, *Astrophys. J.* **564**, 60 (2002).
 - [30] A. H. G. Peter, M. Rocha, J. S. Bullock, and M. Kaplinghat, [arXiv:1208.3026](https://arxiv.org/abs/1208.3026).

- [31] M. Markevitch, A. H. Gonzalez, D. Clowe, A. Vikhlinin, W. Forman, C. Jones, S. Murray, and W. Tucker, *Astrophys. J.* **606**, 819 (2004).
- [32] S. W. Randall, M. Markevitch, D. Clowe, A. H. Gonzalez, and M. Bradac, *Astrophys. J.* **679**, 1173 (2008).
- [33] J. P. Ostriker, *Phys. Rev. Lett.* **84**, 5258 (2000).
- [34] J. F. Hennawi and J. P. Ostriker, [arXiv:astro-ph/0108203](https://arxiv.org/abs/astro-ph/0108203).
- [35] O. Y. Gnedin and J. P. Ostriker, [arXiv:astro-ph/0010436](https://arxiv.org/abs/astro-ph/0010436).
- [36] F. J. Sanchez-Salcedo, *Astrophys. J.* **631**, 244 (2005).
- [37] J. Zavala, M. Vogelsberger, and M. G. Walker, *Mon. Not. R. Astron. Soc.* **431**, L20 (2013).
- [38] S. Tulin, H.-B. Yu, and K. M. Zurek, *Phys. Rev. D* **87**, 115007 (2013).
- [39] E. R. Cohen, D. Lide, and G. Trigg, *Physicist's Desk Reference* (Springer, New York, 2003).
- [40] J. L. Feng, M. Kaplinghat, H. Tu, and H.-B. Yu, *J. Cosmol. Astropart. Phys.* **07** (2009) 004.
- [41] W. Bauer, B. Lantzsch, J. P. Toennies, and K. Walaschewski, *Chem. Phys.* **17**, 19 (1976).
- [42] J. Schaefer and W. Meyer, *J. Chem. Phys.* **70**, 344 (1979).
- [43] G. Quémener and N. Balakrishnan, *J. Chem. Phys.* **130**, 114303 (2009).